PhotoniX

RESEARCH Open Access

Observation of single-molecule Raman spectroscopy enabled by synergic electromagnetic and chemical enhancement

Haiyao Yang[1], Haoran Mo[1], Jianzhi Zhang[1], Lihong Hong[1] and Zhi-Yuan Li[1,2*]

*Correspondence:
phzyli@scut.edu.cn

[1] School of Physics and Optoelectronics, South China University of Technology, Guangzhou 510640, China
[2] State Key Laboratory of Luminescent Materials and Devices, South China University of Technology, Guangzhou 510640, China

Abstract

There has been a long fundamental pursuit to enhance and levitate the Raman scattering signal intensity of molecule by a huge number of ~ 14–15 orders of magnitude, to the level comparable with the molecule fluorescence intensity and truly entering the regime of single-molecule Raman spectroscopy. In this work we report unambiguous observation of single-molecule Raman spectroscopy via synergic action of electromagnetic and chemical enhancement for rhodamine B (RhB) molecule absorbed within the plasmonic nanogap formed by gold nanoparticle sitting on the two-dimensional (2D) monolayer WS_2 and 2 nm SiO_2 coated gold thin film. Raman spectroscopy down to an extremely dilute value of 10^{-18} mol/L can still be clearly visible, and the statistical enhancement factor could reach 16 orders of magnitude compared with the reference detection sample of silicon plate. The electromagnetic enhancement comes from local surface plasmon resonance induced at the nanogap, which could reach ~ 10–11 orders of magnitude, while the chemical enhancement comes from monolayer WS_2 2D material, which could reach 4–5 orders of magnitudes. This synergic route of Raman enhancement devices could open up a new frontier of single molecule science, allowing detection, identification, and monitor of single molecules and their spatial–temporal evolution under various internal and external stimuli.

Introduction

Raman spectroscopy is a traditional and powerful means to observe vibrational, rotational, and other low-frequency modes in materials via inelastic scattering against light, and enable molecule and material analysis and identification [1–7]. After 90 years of development, it still attracts tremendous interest to probe single-molecule (SM) Raman spectroscopy, which is not just an ultrasensitive version of traditional Raman spectroscopy, but rather opens up a new window to observe subtle spectroscopic phenomena in single molecules without statistical average, enabling much more clarified observation of molecule science details [8–11]. The enhancement factor (EF) of Raman spectra, which a critical quantity for Raman spectroscopy, is the ratio of Raman signal with and without substrates in the same experimental environment, normalized for the number of molecules probed:

$$EF = \frac{I_E/N_{surf}}{I_R/N_{vol}} \tag{1}$$

where I_R and I_E are the Raman intensity for N_{vol} molecules and enhanced Raman intensity for N_{surf} molecules, respectively. Since Nie, Kneipp and their co-workers claimed SM Raman detection for the first time in 1997 [11, 12], and Xu's team reported a 10^{10} EF for single hemoglobin molecule in 1999 [13], all through the scheme of surface-enhanced Raman spectroscopy (SERS) mediated by surface plasmon polariton (SPP) excitation and action, multiple researches paving towards the road of SM-SERS have been accomplished [14–24], among these, the highest EF is 10^{12} [21, 25].

It is generally acknowledged that Raman signal needs a huge EF of ~ 14–15 orders of magnitude to maintain a signal intensity comparable with molecule fluorescence, which allows one to truly enter the regime of single-molecule detection sensitivity [11, 12]. This criterion has set a huge obstacle to frustrate and obstruct most contemporary macroscopic, mesoscopic, and microscopic strategies of Raman scattering enhancement [7], including two most prestigious schemes, the electromagnetic enhancement (EME) and chemical enhancement (CME) [26–28]. EME is mainly induced by mesoscopic local surface plasmon resonance (LSPR) effect in metallic nanoparticles and nanostructures with their free electron gas violently interacting with incident laser light, leading to occurrence of great electric field intensity and Raman enhancement in specific nanoscale regions called hot spot [29, 30]. CME is mainly a microscopic effect where the molecule Raman cross section (or Raman activity) is enlarged by the formation of loose chemical bond between molecule and surrounding background and consequent action of additional pathways of charge-transfer resonance [30, 31].

The above argument can be placed into a more clarified physical model. The signal intensity of enhanced Raman scattering is expressed as.

$$I(\omega_R) = \{AI_0(r_0,\omega)\} \times |\alpha(\omega_R,\omega)|^2 \times \left\{\frac{|E(r_0,\omega)|^4}{|E_0(r_0,\omega)|^4}\right\}, \tag{2}$$

where A is a coefficient related in practice with the collection efficiency of the optical system used to collect the Raman signal, $I_0(r_0,\omega)$ is the intensity of incident light, $\alpha(\omega_R,\omega)$ is the Raman polarizability (proportional to Raman activity or cross section), of the detected molecule, and $\frac{|E(r_0,\omega)|^4}{|E_0(r_0,\omega)|^4}$ corresponds to the famous local field enhancement factor [9]. Equation (2) has implied that one can harness the macroscopic strategy of Raman instrument improvement (first term), the microscopic strategy of molecule Raman polarizability enhancement (second term, CME), and the mesoscopic strategy of local field enhancement (third term, EME) to push up the overall enhancement of Raman detection down to single-molecule (SM) level. Since the space for macroscopic instrument performance improvement is very limited, one should focus to dig into mesoscopic EME and microscopic CME for SM Raman detection. Previous studies have shown that EME can become large in SERS substrates made from noble metal Au and Ag single nanoparticles with sharp tips, corners, and edges [32, 33], or nanoparticle dimers or aggregates with nanoscale gap between them [34–36], or in TERS configuration with a sharp Ag/Au tip sitting above planar Ag/Au substrates [37–39]. So far, the biggest EME occurs in Ag/Au nanoparticle dimers or aggregates, which can reach 10–11

orders of magnitude, still 3–5 orders of magnitude shorter than the SM detection limit. Compared with EME, CME achieves a relatively low enhancement factor. In usual Ag/Au nanoparticle SERS substrates, CME is present together with EFE, but the magnitude is only 10–100. In some carbon nano-porous substrates [40], CME can reach a very high value of 10^6, but unfortunately, the CME is negligibly small here. It is clear that either EME or CME alone is unable to make SM Raman detection, but synergic action of simultaneous strong EME and CME might be feasible to bring reality the dream of SM Raman detection.

In this work we harness both EME and CME to reach a very high level of Raman enhancement simultaneously. We successfully design and implement a 2D material-plasmon nanogap composite nanoscale system and make unambiguous experimental observation of single-molecule Raman spectroscopy of RhB molecule. The RhB molecules are absorbed on two-dimensional monolayer WS_2 sheets, within the plasmonic nanogap formed by gold nanoparticle sitting upon 2 nm SiO_2 coated gold thin film on a 5mm × 5mm square silicon wafer as shown in Fig. 1. Raman spectroscopy down to an extremely dilute value of 10^{-18} mol/L can be clearly visible, and the statistical enhancement factor could reach 16 orders of magnitude compared with the reference detection sample of silicon plate with a detection limit of 10^{-2} mol/L. The electromagnetic enhancement comes from local plasmon resonance induced at the nanogap, which could reach ~ 10–11 orders of magnitude, while the chemical enhancement comes from monolayer WS2 2D material, which could reach 4–5 orders of magnitudes.

Results

The first step to confirm the power of our SM-SERS strategy is to find a good 2D material exhibiting strong CME. We proceeded a series of tests on Mxenes, black phosphorus and transition-metal dichalcogenides (TMDCs), which are promising to have Raman

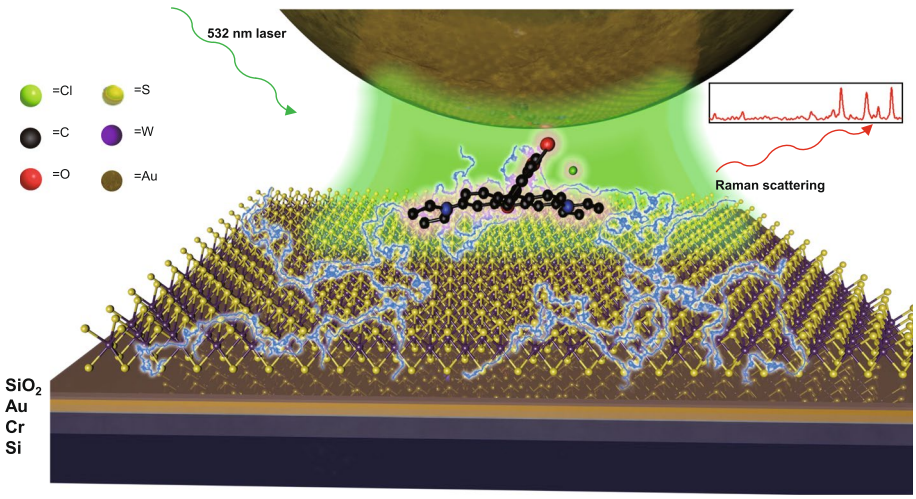

Fig. 1 Schematic diagram of RhB SM-SERS Raman detection. The golden sphere on the top refers to the attached Au nanoparticle. The green region below is the hot spot of excitation laser. The black (carbon), mazarine (nitrogen) and red (oxygen) ball-and-stick model presents the RhB molecule. The yellow (sulfur) and violet (tungsten) ball-and-stick model shows the mono-layer WS_2. The blue flash pattern illustrates the charge transfer between the RhB molecule and mono-layer WS_2. The subjacent cuboid shows the silicon slice with several coatings

enhancement. A kind of TMDCs WS_2 is proved to be capable of $10^4 \sim 10^5$ Raman magnification for RhB, while the other tested materials did not show enhancement factor higher than 10^2, so we estimate WS_2 as the most promising CME substance for RhB SM Raman probing. RhB molecules are attached on monolayer WS_2, and afterwards laid on a 2 nm SiO_2 coated gold thin film. Finally, gold nanoparticles are added to form nanogap with the Au plating (Fig. 2a). Optical microscope image shows the tight attachment of WS_2 slices on the base (Fig. 2b), and scanning electron microscopy (SEM) picture in Fig. 2c indicates that the Au nano-particles are distributed barely evenly on the monolayer WS_2 (each with area of one square micrometer). The low wave number Raman spectra as illustrated in Fig. S4b indicates that the WS_2 sheet in the working hot spot is monolayer as the intensity of 356 cm^{-1} ($E^1_{2g}(\Gamma)$) is higher than 417.5 cm^{-1} ($A_{1g}(\Gamma)$) [41]. Energy dispersive spectroscopy (EDS) elemental mapping clearly demonstrates that the tungsten element is distributed on the gold film uniformly (Fig. 2d), in another word, the monolayer WS_2 is uniformly attached to the base [42].

The spectra in Fig. 3 illustrates the CME effect of monolayer WS_2 for RhB with various concentrations, which indicate the lowest detectable threshold of pure RhB is 10^{-2} M in a silicon substrate with neither EME nor CME for Raman scattering. With the aid of the WS_2 CME, the detection limit of RhB molecule can reach 10^{-7} M, meanwhile the Raman intensity of 10^{-6} M RhB on WS_2 is of same order of magnitude with 10^{-2} M sole RhB on silicon wafer. Thus, the CME factor of monolayer WS_2 can be defined as $10^4 \sim 10^5$.

CME for WS_2 based SERS is dependent on the electronic structure of the interface between the RhB molecules and the WS_2, therefore the molecules layer closest by the substrate is the key crucial to CME, which is generally defined as "first layer effect" [43]. The RhB molecule contains a chloride anion and a cation framework, thus the molecule

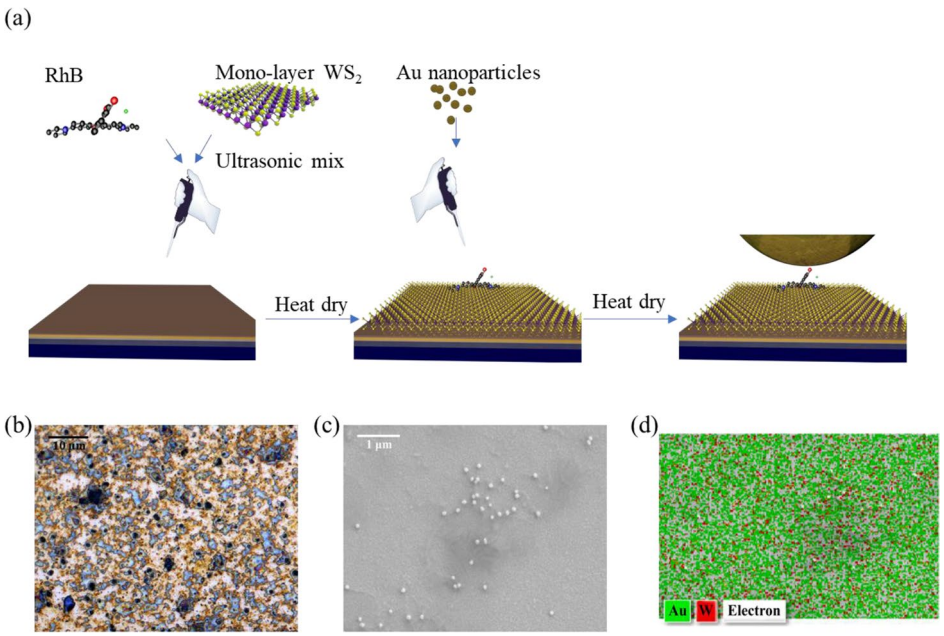

Fig. 2 Fabrication and micromorphology of RhB SM Raman base. **a** Preparation progress of the sample. **b** Optical microscope and (**c**) SEM image of the base surface. **d** EDS elemental mapping of the gold nanoparticle on the base

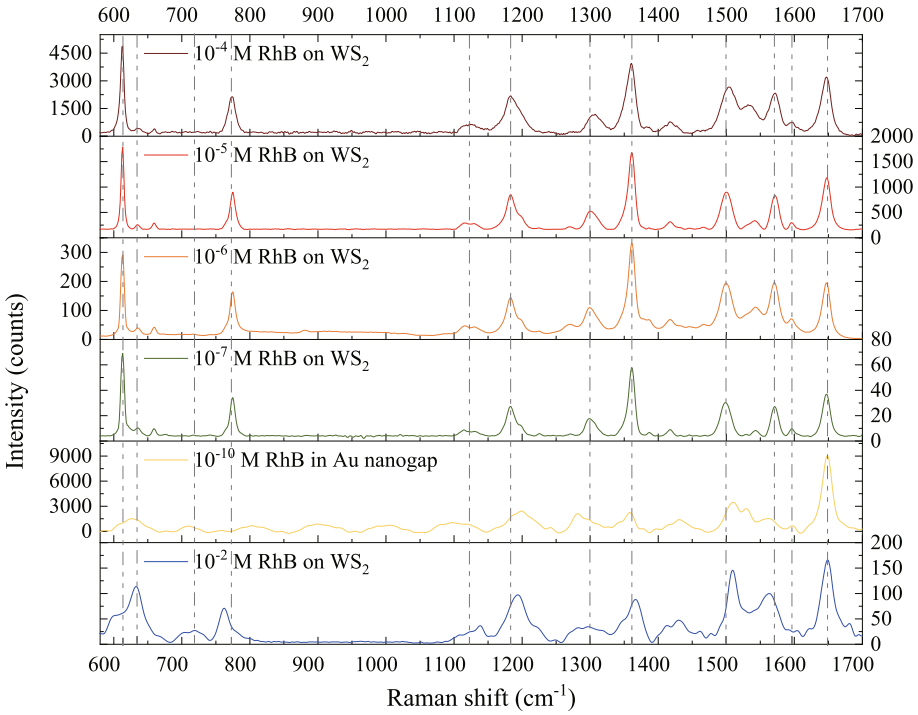

Fig. 3 Experimental characterization of WS_2 chemical enhancement and Au plasmonic nanogap electromagnetic enhancement for RhB Raman scattering. From top to bottom panels show the WS_2 enhanced (brown, red, orange and green lines) Raman spectra, Au nanogap enhanced Raman spectra (yellow line) and normal Raman spectra of RhB (blue line)

frameworks can attach tightly to the WS_2, which has abundant negative charge on the surface. Moreover, the charge transfer (CT) mechanism tends to appear between the adsorbed RhB molecules and WS_2 mono-layer material. On the basis of frontier molecular orbital theory, the electrons with different energies in molecules will be assigned into different molecular orbital energy levels [44], among which the highest occupied molecular orbital (HOMO) and the lowest unoccupied molecular orbital (LUMO) are dominating in the interaction with other matters [45, 46]. As discussed in Supplementary Information S1, the calculated molecular orbitals of RhB and energy band of monolayer WS_2 indicates that the valence band of WS_2 is totally included between the HOMO and LUMO of RhB. As a result, charge carriers in the valence band can provide charges to the HOMO through charge transfer (CT), and enhance LUMO via CT resonance in the meantime (Supplementary Information, Figs. S1 and S2). The extremely high carrier mobility of WS_2 (Supplementary Information, Table S1) further amplifies the effect of CT and CT resonance, so that finally a CME of $10^4 \sim 10^5$ can be achieved [47–50].

Because of the charge transfer between the RhB molecules and WS_2, several peaks in the WS_2 enhanced Raman spectra of RhB fluctuate or/and shift compared with the normal spectrum, which are declared by grey dashed lines in Fig. 3. Let "X" represents the xanthene ring, "M" represents the methyl, and "D" represents the diethylamino group, respectively. WS_2 enhanced Raman spectra of RhB differ from the ordinary spectrum in the following details. The bands of C_X–C_X–C_X bending vibrations are not shifted to different wavenumbers, while the broad band at 613 cm^{-1} turns to an

extremely narrow and strong peak and the band at 632 cm^{-1} decreases dramatically. In the case of the C_X–H in-plane bending vibrations, the band at 717 cm^{-1} almost disappears, the band at 1136 cm^{-1} gets weaker and shifts to the lower wavenumbers. In the mean time, the band at 761 cm^{-1} standing for C_X–H out-of-plane bend is shifted to higher wavenumbers at 773 cm^{-1}, while the C_X–C_X stretching vibrations (1193, 1367, 1510, 1560 cm^{-1}) are shifted to lower wavenumbers (1182, 1359, 1499, 1542 cm^{-1}). Meanwhile the C_X–N stretching band appears around 1389 cm^{-1}. The above results suggest the spatial orientation reform of the RhB molecule to the WS_2 substrates, and CT enhancement takes place on the interface [51]. It can be explained that the "X" is approximately parallel to the surface when RhB is adsorbed on WS_2, hence, the C_X–C_X stretching bands are highly enhanced other than the C_X–N stretching band and the C_X–H bending vibrations [52].

Figure 3 also displays a typical experimental result of the EME effect for the Au plasmonic nanogap against Raman scattering for RhB molecule. The yellow curve in the fifth panel of Fig. 3 indicates that the EME factor of RhB by the LSPR excited within the Au nanogap nanocavity can reach a very high level of about 4.5 x 10^9. For a more quantitative comparison and justification, we have carried out three-dimensional finite-difference time-domain (3D-FDTD) simulations to evaluate the electromagnetic enhancement factors with and without the WS_2 layer and the RhB molecule. The results are discussed in details in Supplementary Information S2. The simulation results show that the existence of WS_2 layer can enhance the effect of local electromagnetic field, so can the Rhodamine B molecule. Summarily, the maximum electromagnetic enhancement factor can approach to the order of 10^9 according to the FDTD simulations. However, in practical situations, the maximum EF values have the capacity to reach an even larger orders of magnitude when taking into account more complex sample surface and optical field pattern under experiment conditions. For instance, the roughness and shape anomaly of the gold nanoparticles and plating could lead to a larger EME. Besides, molecular Raman polarizability could become higher due to the quantum confinement from WS_2 film and nano-gap upon RhB molecule. Consequently, the overall EME factor can be levitated up to the level of 10^{10}–10^{11}. In fact, this physical picture has been supported to some extent by the comparison between experiment and theory for pure Au nanogap EME without WS_2 incorporated. Notice that the experimental EME factor can reach 4.5 x 10^9, while the theoretical EME factor is at least one order of magnitude lower. If one considers possible larger Raman polarizability of RhB molecule under tight quantum confinement within the nanogap, the calculated EME factor may increase to some extent and better match the experimental EME factor.

The above results reveal that with matched 2D semiconductor materials, the Raman signal of molecule can be amplified 10^5 times due to the chemical interaction between substances, known as the CME of SERS. Whereas the EME mechanism does not rely on the microscopic-level light-matter interactions, it is more like an environment construction: noble metallic nanoparticles and nanostructures form nanogaps with hot spots, where enormous electric field intensity and Raman enhancement take place in this specific nanoscale regions due to the LSPR [53, 54]. Thus, through appropriate combination, the CME and EME can make a synergy to gain single-molecule level Raman detection power. A series of control-experiments is carried out to verify the feasibility.

The experiments illustrating the SM-SERS power for the Au nanaogap-WS_2 2D material substrate are taken on 5 mm × 5 mm chips for each sample. Every chip is added by 30 μL RhB solution with different concentrations. When the concentration reaches down to 10^{-18} M, there are only 18 molecules on one chip on average. The distribution of Au nanoparticles in samples with gold nanogap is about one every square micron. The scanning scope for the samples is 40 μm × 60 μm, the sampling step is 1 μm. The diameter of facula area is easily calculated as 1.298 μm. The weakest detected Raman signal of $10^{-6} \sim 10^{-20}$ M RhB samples are shown in Fig. 4a, which obviously indicates that with the lowest concentration detection limit as 10^{-18} M, the 2D WS_2 material incorporated gold nanogap SERS substrates have successfully entered the realm of SM Raman detection.

It is noteworthy that under ultra-low concentrations, even when the amount of total molecules is increasing, the Raman signal remains in the SM level. This is because only the molecules which have obtained both EME and CME simultaneously can be detected. Besides, as the above results have shown, the detection limit of CME is just 10^{-7} M, and within the incident laser region, there is only one EME hot spot which can contain just an individual RhB molecule [12]. Therefore, when the RhB concentration reaches 10^{-6} M, the signal intensity begins to grow and the value is approximately equal to the sum of former-mentioned SM signal and 10^{-6} M RhB on WS_2 in Fig. 3, as the other exposed molecules initiate to contribute observable Raman signal together with the single molecules sitting inside the hot-spot. A 40 μm × 60 μm range in the center of each sample is scanned, and the achieved Raman mapping pictures of the intensity at 1650 cm^{-1} peak are exhibited in Fig. 4b. Furthermore, the whole chip of 10^{-20} M sample is completely scanned, and no signal could be detected. When the quantity of molecules rises, the amount of active hot spot also increases to induce more SM signals. Taken together, by the synergy of CME and EME, unambiguous RhB SM Raman detection has

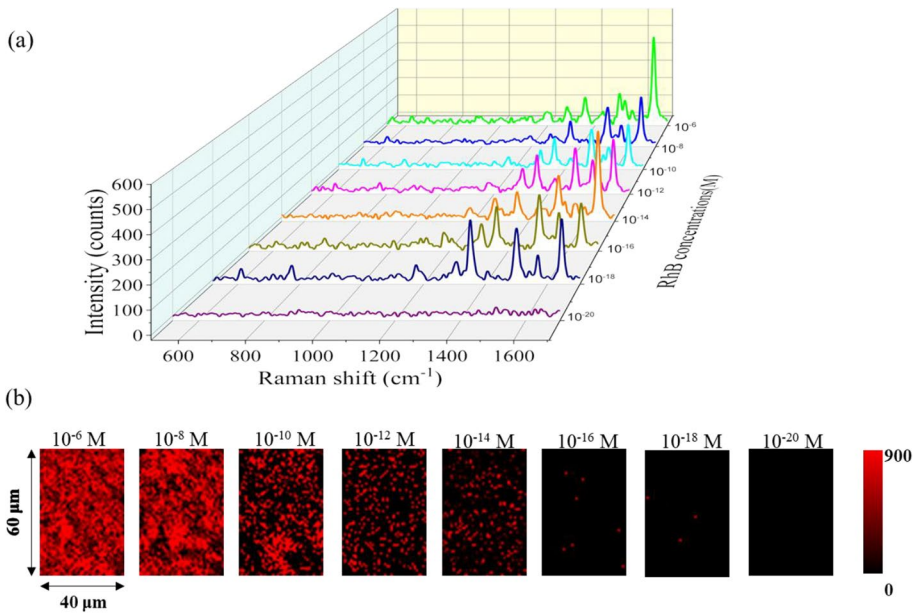

Fig. 4 Experimental characterization of SM-SERS substrate. **a** Raman spectra of RhB with variable concentration in SM Raman base. **b** Raman mapping of the intensity at 1650 cm^{-1} peak of RhB at concentrations $10^{-6} \sim 10^{-20}$ M

been achieved. Under extremely low concentration, RhB molecules are dispersed in the form of single molecule. Because the LSPR in nanogap only occurs in a small region for only a single molecule, Raman signal detected in low concentration samples can only be attributed to SM signals. Meanwhile, the increase of molecule amount will result in more active hot spots to take action and thus more intense Raman signal to be detected. As discussed in Supplementary Information S3, we have compared the Raman mapping picture and the corresponding photomicrograph (Fig. S4a as an example), and confirmed that a particle sitting right upon the molecule absorbed WS_2 is the essential requirement to achieve SM-SERS signal, in another word, the synergy effect of EME and CME is vital to SM-SERS. To further verify the repeatability of our method, we randomly chose two points on several samples with signal detected. The detected curves are shown in Fig. S4b. The signal to noise ratio (Fig. S4c) of these curves are calculated as the ratio of the mean value to the standard deviation of them, which is fluctuating between $6 \sim 8.5$.

Discussion

In conclusion, we have dug deeply into the two major enhancement mechanism for SERS, the EME and CME, explored to maximize the strength of each mechanism, and more importantly, and found out the optimal synergetic action of them, in a hope to fulfill the condition of SM Raman detection. We have found experimentally that 2D material monolayer WS_2 offers a very promising CME with enhancement factor up to 10^5 for absorbed RhB molecules, due to strong CT and CT resonance between the high-mobility WS_2 substrate and RhB molecules. Besides, it is well-established that the plasmonic nanogap made from gold nanoparticles sitting on the gold thin film can offer a very promising EME with enhancement factor up to 10^{10} for molecules absorbed within the nanogap hot spot under an appropriate gap separation size. We have designed and implemented a hybrid configuration of plasmonic nanogap formed by a gold nanoparticle sitting on the 2D monolayer WS_2 and 2 nm SiO_2 coated gold thin film, which in principle should enable synergic action of EME and CME with their individual enhancement factors multiplied. Indeed, our experiments have unambiguously shown that Raman spectroscopy for RhB molecules absorbed on the hybrid plasmonic nanogap can still be clearly observed with an extremely low concentration down to 10^{-18} mol/L, and has successfully entered the realm of SM Raman spectroscopy. The statistical enhancement factor could reach an unprecedented high value as $\sim 10^{16}$ for this hybrid nano-device when compared with the reference detection sample of silicon plate. Moreover, the designed and implemented SM Raman base with so outstanding power of SM detection is very easy to fabricate. Thus, further researches on different molecules and applications are promising. Such a synergic route of Raman enhancement devices could open up a new frontier of single molecule science, allowing detection, identification, and monitor of single molecules and their spatial–temporal evolution under various internal and external stimuli.

Method

Materials

Rhodamine B is obtained from Shanghai Adamas Reagent Co., Ltd. Mono-layer WS_2 dispersion is purchased from Nanjing MKNANO Tech. Co., Ltd. Gold nanoparticle

colloid is achieved from Nanjing XFNANO Materials Tech Co., Ltd. The gold, chromium and SiO_2 sputtering target are acquired from Beijing Dream Material Technology Co., Ltd. All reagents are of analytical grade and used directly without further purification. Deionized water is produced through a Millipore water purification system (Milli-Q, Millipore) and used throughout the study.

Instruments and measurements

The SEM image and EDS elemental mapping are taken by a GemniSEM 500 electron microscope. The HR-TEM images are recorded using a JEOL-2010 electron microscope. The gold, chromium and SiO_2 coating on the SM Raman base are sputtered by an MSP-300B magnetron sputtering instrument. The thickness of coatings is measured by a Bruker DektakXT step profiler. All the Raman spectra are gained from a Renishaw inVia Raman spectrometer, laser: 532 nm edge (mode: Confocal), grating: 2400 l/mm (vis), exposure time for each point: 0.5 s, laser power: 2.5 mW, slit opening 20 μm, objective × 50 L.

Fabrication of the RhB SM Raman base

20 nm chromium, 300 nm gold and 2 nm SiO_2 are sputtered on a 5 mm × 5 mm square silicon slice, successively. 0.2 mL WS_2 (0.1 mg/mL) dispersion is mixed with 2.8 mL RhB solution with specific concentration, the mixture is ultrasonic stirred for 30 min to make the RhB molecules absorbed adequately by the 2D material. Afterwards, 20 μL of the mixture is dropped uniformly on the coated slice. after 2 h vacuum drying under 40 °C, 20 μL gold nanoparticle (6 μg/mL) colloid is added on the aforementioned slice. Eventually, via 2 h vacuum drying beyond 40 °C, the RhB SM Raman base can be created.

Fabrication of the reference samples

RhB solutions with specific concentration is ultrasonic stirred for 30 min. Afterwards, 20 μL of the solutions are dropped uniformly on bare silicon plate. Finally, the samples are 2 h vacuum dried under 40 °C.

Abbreviations

CME	Chemical enhancement
EME	Electromagnetic enhancement
EF	Enhancement factor
2D	Two-dimensional
RhB	Rhodamine B
SM	Single molecule
SERS	Surface-enhanced Raman spectroscopy
SPP	Surface plasmon polariton

Supplementary Information

The online version contains supplementary material available at https://doi.org/10.1186/s43074-024-00119-6.

Supplementary Material 1.

Acknowledgements

Not applicable.

Authors' contributions

Z. Y. Li supervised the project. Z. Y. Li and H. Y. Yang conceived and designed the experiments, H. Y. Yang prepared the samples and performed the experiments, L. H. Hong offered technical assistance, H. R. Mo and J. Z. Zhang offered

assistance in theoretical calculations. H. Y. Yang and Z. Y. Li provided the theoretical and experimental analysis, and wrote the manuscript. All authors participated in the discussion of results and reviewed the manuscript.

Funding
This work is supported by the National Natural Science Foundation of China (11974119), Science and Technology Project of Guangdong (2020B010190001), Guangdong Innovative and Entrepreneurial Research Team Program (2016ZT06C594), and National Key R&D Program of China (2018YFA 0306200).

Availability of data and materials
The data that support the findings of this study are available from the corresponding author on request.

Declarations

Ethics approval and consent to participate
There is no ethics issue for this paper.

Consent for publication
All authors agreed to publish this paper.

Competing interests
The authors declare that they have no competing interests.

Received: 2 November 2023 Revised: 8 December 2023 Accepted: 20 February 2024
Published online: 29 February 2024

References

1. Ferrari AC. Basko. Raman spectroscopy as a versatile tool for studying the properties of graphene. Nat Nanotechnol. 2013;8:235.
2. Kneipp K, Kneipp H, Itzkan I, Dasari RR. Feld. Ultrasensitive chemical analysis by Raman spectroscopy. Chem Rev. 1999;99:2957.
3. Andrews DH. The relation between the raman spectra and the structure of organic molecules. Phys Rev. 1930;36: 544.
4. Ramaswamy C. Raman effect in diamond. Nature. 1930;125:704.
5. Kerker M, Wang DS, Chew H. Surface enhanced Raman scattering (SERS) by molecules adsorbed at spherical particles. Appl Opt. 1980;19: 3373.
6. Long L, Ju W, Yang HY, Li Z. Dimensional design for surface-enhanced raman spectroscopy. ACS Mater Au. 2022;2:552.
7. Li ZY. Mesoscopic and microscopic strategies for engineering plasmon-enhanced raman scattering. Adv Opt Mater. 2018;6(16):1701097.
8. Qiu Y, Kuang C, Liu X. Tang. Single-molecule surface-enhanced Raman Spectroscopy. Sens (Basel). 2022;22:4889.
9. Yu Y, Xiao TH, Wu YZ, et al. Roadmap for single-molecule surface-enhanced raman spectroscopy. Adv Photonics. 2020;2:014002.
10. de Virgilio M, Weninger H, Ivessa NE. Ubiquitination is required for the retro-translocation of a short-lived luminal endoplasmic reticulum glycoprotein to the cytosol for degradation by the proteasome. J Biol Chem. 1998;273:9734.
11. Kneipp K, Wang Y, Kneipp H, et al. Single molecule detection using surface-enhanced Raman scattering (SERS). Phys Rev Lett. 1997;78:1667.
12. Nie S. Emory. Probing single molecules and single nanoparticles by Surface-Enhanced Raman Scattering. Science. 1997;275:1102.
13. Xu HX, Bjerneld EJ, Kall M, Borjesson L. Spectroscopy of single hemoglobin molecules by surface enhanced Raman scattering. Phys Rev Lett. 1999;83:4357.
14. Xia C, Zhang D, Li H, et al. Single-walled carbon nanotube based SERS substrate with single molecule sensitivity. Nano Res. 2021;15:694.
15. Shingaya Y, Takaki H, Kobayashi N, Aono M, Nakayama T. Single-molecule detection with enhanced Raman scattering of tungsten oxide nanostructure. Nanoscale. 2022;14:14552.
16. Jaculbia RB, Imada H, Miwa K, et al. Single-molecule resonance Raman effect in a plasmonic nanocavity. Nat Nanotechnol. 2020;15:105.
17. Zong C, Premasiri R, Lin H, et al. Plasmon-enhanced stimulated Raman scattering microscopy with single-molecule detection sensitivity. Nat Commun. 2019;10:5318.
18. Sugano K, Aiba K, Ikegami K, Isono Y. Single-molecule surface-enhanced Raman spectroscopy of 4,4′-bipyridine on a prefabricated substrate with directionally arrayed gold nanoparticle dimers. Jpn J Appl Phys. 2017;56:06gk01.
19. Zheng Y, Soeriyadi AH, Rosa L, et al. Reversible gating of smart plasmonic molecular traps using thermoresponsive polymers for single-molecule detection. Nat Commun. 2015;6:8797.
20. Darby BL, Etchegoin PG, Le Ru EC. Single-molecule surface-enhanced Raman spectroscopy with nanowatt excitation. Phys Chem Chem Phys. 2014;16:23895.
21. Li L, Hutter T, Steiner U, Mahajan S. Single molecule SERS and detection of biomolecules with a single gold nanoparticle on a mirror junction. Analyst. 2013;138:4574.
22. McGuinness CD, Macmillan AM, Karolin J, et al. Single molecule level detection of allophycocyanin by surface enhanced resonance Raman scattering. Analyst. 2007;132:633.

23. Zhou ZH, Wang GY, Xu ZZ. Single-molecule detection in a liquid by surface-enhanced resonance Raman scattering. Appl Phys Lett. 2006;88:034104.
24. Maher RC, Dalley M, Le Ru EC, et al. Physics of single molecule fluctuations in surface enhanced Raman spectroscopy active liquids. J Chem Phys. 2004;121:8901.
25. Lin CL, Liang SS, Peng YS, et al. Visualized SERS Imaging of single molecule by Ag/Black phosphorus nanosheets. Nano-Micro Lett. 2022;14:75.
26. Fan M, Andrade GFS, Brolo AG. A review on recent advances in the applications of surface-enhanced Raman scattering in analytical chemistry. Anal Chim Acta. 2020;1097:1.
27. Langer J, Jimenez de Aberasturi D, Aizpurua J, et al. Present and Future of Surface-enhanced Raman Scattering. ACS Nano. 2020;14:28.
28. Zrimsek AB, Chiang N, Mattei M, et al. Single-Molecule Chemistry with Surface- and Tip-Enhanced Raman Spectroscopy. Chem Rev. 2017;117:7583.
29. Kleinman SL, Sharma B, Blaber MG, et al. Structure enhancement factor relationships in single gold nanoantennas by surface-enhanced Raman excitation spectroscopy. J Am Chem Soc. 2013;135:301.
30. Wang X, Huang SC, Hu S, Yan S, Ren B. Fundamental understanding and applications of plasmon-enhanced Raman spectroscopy. Nat Reviews Phys. 2020;2:253.
31. Ling X, Fang W, Lee YH, et al. Raman enhancement effect on two-dimensional layered materials: graphene, h-BN and MoS2. Nano Lett. 2014;14:3033.
32. Beams R, Gustavo Cancado L, Novotny L. Raman characterization of defects and dopants in graphene. J Phys Condens Matter. 2015;27: 083002.
33. Neumann C, Reichardt S, Venezuela P, et al. Raman spectroscopy as probe of nanometre-scale strain variations in graphene. Nat Commun. 2015;6:8429.
34. Li JF, Tian XD, Li SB, et al. Surface analysis using shell-isolated nanoparticle-enhanced Raman spectroscopy. Nat Protoc. 2013;8:52.
35. Wei RB, Kuang PY, Cheng H, et al. Plasmon-enhanced Photoelectrochemical Water Splitting on Gold Nanoparticle decorated ZnO/CdS nanotube arrays. ACS Sustain Chem Eng. 2017;5:4249.
36. Yin Z, Wang Y, Song C, et al. Hybrid Au-Ag nanostructures for enhanced Plasmon-Driven Catalytic Selective Hydrogenation through visible light irradiation and surface-enhanced Raman Scattering. J Am Chem Soc. 2018;140:864.
37. Pettinger B, Schambach P, Carlos J Villagómez, et al. Tip-Enhanced Raman Spectroscopy: Near-fields acting on a few molecules. Annu Rev Phys Chem. 2012;63(1):379–99.
38. Pienpinijtham P, Kitahama Y, Ozaki Y. Electric field analysis, polarization, excitation wavelength dependence, and novel applications of tip-enhanced Raman scattering. J Raman Spectrosc. 2021;52:1997.
39. Zhang KF, Taniguchi S, Saeki T, et al. Simple cleaning and regeneration of tip-enhanced Raman spectroscopy probe with UV sources. J Raman Spectrosc. 2022;53:2023.
40. Xiao TH, Cheng Z, Luo Z, et al. All-dielectric chiral-field-enhanced Raman optical activity. Nat Commun. 2021;12:3062.
41. Berkdemir A, Gutiérrez HR, Botello-Méndez AR, et al. Identification of individual and few layers of WS2 using Raman Spectroscopy. Sci Rep. 2013;3:1755.
42. Shi W, Lin ML, Tan QH, et al. Raman and photoluminescence spectra of two-dimensional nanocrystallites of monolayer WS2 and WSe2. 2d Materials. 2016;3:025016.
43. Zhang N, Tong LM, Zhang J. Graphene-based enhanced Raman scattering toward Analytical Applications. Chem Mater. 2016;28:6426.
44. Fukui K, Yonezawa T, Shingu H. A molecular Orbital theory of reactivity in aromatic hydrocarbons. J Chem Phys. 1952;20:722.
45. Yin Y, Miao P, Zhang Y, et al. Significantly increased Raman Enhancement on MoX2 (X = S, Se) Monolayers upon Phase Transition. Adv Funct Mater. 2017;27(16):1606694.
46. Xu H, Xie L, Zhang H, Zhang J. Effect of graphene Fermi level on the Raman scattering intensity of molecules on graphene. ACS Nano. 2011;5:5338.
47. Ming X. A Review on applications of two-dimensional materials in surface-enhanced Raman Spectroscopy. Int J Spectrosc. 2018;4861472:9.
48. Shutov AD, Yi Z, Wang J, et al. Giant Chemical Surface Enhancement of Coherent Raman scattering on MoS2. ACS Photonics. 2018;5:4960.
49. He R, Lai H, Wang S, et al. Few-layered vdW MoO3 for sensitive, uniform and stable SERS applications. Appl Surf Sci. 2020;507: 145116.
50. Wu Z, Zeng P, Zhao W, et al. Synthesis of single- and few-Layer Nitrogen-doped Graphene and Layer-Dependent Surface-enhanced Raman Scattering properties. J Phys Chem C. 2021;125:17831.
51. Wang Z, Rothberg LJ. Origins of blinking in single-molecule Raman spectroscopy. J Phys Chem B. 2005;109:3387.
52. Saini GS, Kaur S, Tripathi SK, et al. Spectroscopic studies of rhodamine 6G dispersed in polymethylcyanoacrylate. Spectrochim Acta Mol Biomol Spectrosc. 2005;61:653.
53. Wang HL, You EM, Panneerselvam R, Ding SY. Tian. Advances of surface-enhanced Raman and IR spectroscopies: from nano/microstructures to macro-optical design. Light Sci Appl. 2021;10:161.
54. Dong X, Yang B, Zhu R, et al. Tip-induced bond weakening, tilting, and hopping of a single CO molecule on Cu(100). Light Adv Manuf. 2022;3:729–38.

Publisher's Note